

16p



A NEW HIGHLY LUMINOUS MASS SPECTROMETER FOR MEASURING  
THE COMPOSITION OF THE UPPER ATMOSPHERE

Dr. J. Geerk

FACILITY FORM 602	N66 29429	(THRU)
	(ACCESSION NUMBER)	1
	16 (PAGES)	(CODE)
	(NASA CR OR TMX OR AD NUMBER)	14 (CATEGORY)

Translation of: "Ein neues lichtstarkes Massenspektrometer zur Messung der Zusammensetzung der hohen Atmosphäre". Deutsch-Französisches Forschungsinstitut Saint-Louis. Technische Mitteilung T 8/61, 12 pp. of text plus 8 pp. of illustrations. June 29, 1962. (Unpublished MS).

NATIONAL AERONAUTICS AND SPACE ADMINISTRATION  
WASHINGTON

April 1964

NASA TT F-8857

GPO PRICE \$ \_\_\_\_\_

CFSTI PRICE(S) \$ \_\_\_\_\_



Hard copy (HC) 1.00

Microfiche (MF) .50

French-German Research Institute  
Saint-Louis

Technical Note T 8/61

A New Highly Luminous Mass Spectrometer for Measuring  
the Composition of the Upper Atmosphere

Original Text in German

Saint-Louis, 29 June 1961

Dr. J. GEERK

Chief Engineer R. CASSAGNOU

Directors:

Prof. Dr. Ing. H. SCHARDIN

CONTENTS

Part I	1
Important characteristics of the new mass spectrometer and results of the measurements	1
1. The ion optics of the device	1
2. The dispersion	3
3. The opening error	3
4. The energy blurring error	3
5. The total error	4
6. The aplanatic image	4
7. The ion source	4
8. The mass spectrogram	4
Part II	5
The Veronique Spectrometer	5
1. The physical prototype	5
2. The launchable prototype	5

14229

## ABSTRACT

A

/5

In Part I a description of the device is presented and briefly discussed, i.e., the ion optics, the dispersion, the opening error, the energy blurring error, the total error, the aplanatic image, the ion source, and the mass spectrogram.

In Part II the first prototype, designed for flight with the Veronique, is briefly described with a photograph, and a functional diagram is shown. In addition, a second launchable prototype which can be completely baked is briefly described.

AUTHOR

Part I. Important Characteristics of the New Mass Spectrometer and Results of the Measurements

1. The Ion Optics of the Device

The analyzer under consideration is a homogeneous magnetic field with rectilinear boundaries (Figure 1). First we consider a homocentric, isokinetic ion beam (in Figure 1 designated as the ion source) whose central ray enters the magnetic field at an angle  $\epsilon$  such that  $\tan \epsilon = \frac{1}{2} \sqrt{2}$  and which consists simply of molecules of mass  $m_n$ . Measured along the central ray, the center of the beam is at an arbitrary distance  $l_0$  from the field boundary. The ions of mass  $m_n$  go through the magnetic field along orbits having radii  $r_n$  and return into the field-free space where their orbits are again straight lines. The orbit of an ion of mass  $m_n$  has the radius

/6

$$r_n = \frac{1}{B} \sqrt{2 \frac{m_n}{e} U} ; \quad (1)$$

$B$  = magnetic induction,  $U$  = acceleration voltage of the ions,  $e$  = elementary electric charge.

The ions leaving the field merge not as a homocentric beam but, because of aberration, as a caustic beam. The caustic has a cusp which is traversed by the central ray of the caustic beam. Figure 1 shows only the central ray of the beam under consideration and the caustic. We choose the caustic cusp as the image point of our system, since the opening error is smallest at this point of the caustic. The distance

$l_n$ , to the cusp from the field boundary, again measured along the central ray is calculated from the equation

$$\frac{l_n}{r_n} + \frac{l_0}{r_n} = \frac{2}{3} \sqrt{2} \quad (2)$$

Equation (2) is a result of the telescopic path of the system rays. The system is telescopic since ion rays falling parallel into the magnetic field also leave the field in parallel. Equation (2) is valid as long as the distance between the ion source and the field boundary  $l_0$  is

chosen or adjusted within the limits

$$0 \leq l_0 \leq \frac{2}{3} \sqrt{2} r_n \quad (3)$$

A further result of the telescopic ray path is the constancy of the angular, lateral and longitudinal magnifications when the ion source is moved along the central ray, keeping equations (2) and (3) in mind. All three magnifications are in our case constant and equal to 1. The form of the caustic also remains strictly the same when shifted. /7

Instead of only one ion type, we now let the ion source furnish different ion types of masses  $m_1, m_2, \dots, m_n$ . We then obtain according to equation (1) the radii associated with these masses,  $r_1, r_2, \dots, r_n$ , and according to equation (2) the distances from the caustic cusps  $l_1, l_2, \dots, l_n$ . All cusps are located on a straight line, the straight line of images. On the basis of the geometrical laws of similarity the caustics  $K_1, K_2, \dots, K_n$  are completely similar to each other. If the ion source is shifted along the central ray by a distance  $a$ , the straight line of images, including the invariable caustics, slides parallel to itself by the same distance  $a$ , as measured along the central ray of any caustic. If the ion source is moved toward the field boundary ( $l_0 = 0$ ), the straight line of images goes through the ion source or, in other words, through the center of the homocentric ion beam.

The line of images and the field boundary form the angle  $90^\circ - 2\epsilon$ . The acceptance angles of the caustic central rays are  $= \epsilon$ . The three magnifications are constant for all masses and equal to 1. With the help of equations (1)-(3) and with what has been explained above it becomes /8

possible to construct the whole system of rays. From  $\tan \epsilon = \frac{1}{2} \sqrt{2}$  one obtains  $\epsilon \approx 35^\circ 16'$ .

## 2. The Dispersion

The dispersion coefficient for our system is

$$D = \frac{4}{3} . \quad (4)$$

The mass dispersion  $dp$  is

$$dp = \frac{1}{2} D \cdot r_n \cdot \frac{\Delta m}{m} = \frac{2}{3} r_n \cdot \frac{\Delta m}{m} . \quad (5)$$

$\frac{\Delta m}{m}$  is the relative mass difference of two ion masses whose dispersion  $dp$  is to be calculated.

## 3. The Opening Error

The location of the smallest opening error of the caustic beam does not lie at the cusp itself, but at a small distance  $y_0$  from the cusp on

the central ray, in the direction opposite the particle motion direction. Let  $\alpha_0$  be equal to one half the opening angle of our homocentric beam

when it leaves the ion source; the error calculation results in

$$y_0 = \frac{1}{2} \sqrt{2} \alpha_0^3 r_n . \quad (6)$$

The cage slit must therefore be placed at the distance  $y_0$  from the cusp.

The straight line of images of Figure 1 is, because of this correction, slightly shifted in the direction of the magnetic field. The total opening error at this position is

$$a_y = \frac{1}{3} \sqrt{2} \alpha_0^3 r_n . \quad (7)$$

## 4. The Energy Blurring Error

/9

Since ions are created in the ionization chamber at different locations by the electric attractive field  $\Delta U$ , they have, after traversing the acceleration voltage  $U$ , an energy difference of  $e \cdot \Delta U$ . The resulting error  $a_u$  amounts to

$$a_u = \frac{1}{2} D \frac{\Delta U}{U} r_n = \frac{2}{3} \frac{\Delta U}{U} r_n . \quad (8)$$

## 5. The Total Error

(7) and (8) result in the total error:

$$a = a_o + a_u = \frac{1}{3} r_n (\sqrt{2} \alpha_o^3 + 2 \frac{\Delta U}{U})$$

## 6. The Aplanatic Image

We consider an arbitrary ray S of our homocentric beam. Let ray S and the central ray form the objective ray angle  $\alpha_1$ . In the caustic beam let ray S and the central ray form the image ray angle  $\alpha_2$ . Then  $\alpha_1 = \alpha_2$ .

This leads to an angular magnification  $\alpha_2/\alpha_1 = 1$ , as mentioned above.

All derivatives higher than those of the first order  $\frac{d^k \alpha_2}{d\alpha_1^k} k = 2, 3, \dots$  are zero. It follows that Abbé's sinus law is satisfied. Since the opening error of second order is thus corrected, we call the image of the objective point, i.e., of the beam center, on the straight line of images, the "aplanatic of second order", in accordance with the known Abbé definitions for aplanatism.

## 7. The Ion Source

/10

As ion accelerating system, a system of large angle has been developed with a total opening angle of  $2\alpha_o = 15^\circ$  to  $20^\circ$  (see Technical Note T 4/61).

## 8. The Mass Spectrogram

With the help of a mechanically driven running cage the total mass spectrum was measured without requiring any change in the electric or magnetic parameters. The sharp and well defined mass lines confirm experimentally the accuracy of the theoretically calculated ray system presented in Figure 1. Figure 2 shows the spectrogram of a water vapor-methane, hydrogen mixture which was taken with the help of an oscillograph.

In place of the running cage several fixed cages can be located on the straight line of images for the case where certain masses whose intensities vary with time are to be measured continually.

## Part II. The Veronique Spectrometer

/11

### 1. The Physical Prototype

The spectrometer described in Part I has three advantages which make it suitable - when mounted in a space probe - for measuring the chemical composition of the high atmosphere.

1. The aplanatic image of second order allows for a larger opening angle. The system is therefore very light sensitive, a fact which has in practice been proven by direct comparison with a standard spectrometer.

2. Several masses can be measured continually and simultaneously.

3. None of the electric voltages or magnetic field intensities of the device must be changed during the measurement. The mass spectrometer does not require any relays.

In order to continually measure the components  $O_2$ ,  $N_2$ ,  $O_1$ ,  $N_1$  four detectors are needed. In a first prototype this method was tried with two detectors (see Figure 3). By periodically making small variations of the accelerating voltage the masses  $O_2$  and  $N_2$  were registered by the first detector and the masses  $O_1$  and  $N_1$  were registered in the second, alternately. With a time-variable mixture of air and methane, whereby methane was used to replace the atomic oxygen, and the radical  $CH_2$  was used to replace the atomic nitrogen, it could be shown in a model tested with 120 measuring points per minute, how the spectrometer would work during its flight through the high atmosphere (see Figure 4).

/12

### 2. The Launchable Prototype (see Figure 5 and Figure 6a, b, c)

A second prototype is nearing completion. It differs from the first one in the following points:

1. It is entirely made of nonmagnetic stainless steel and can be completely baked in order to obtain a very good high vacuum.

2. It is mechanically sturdy enough to withstand the expected strong vibrations.

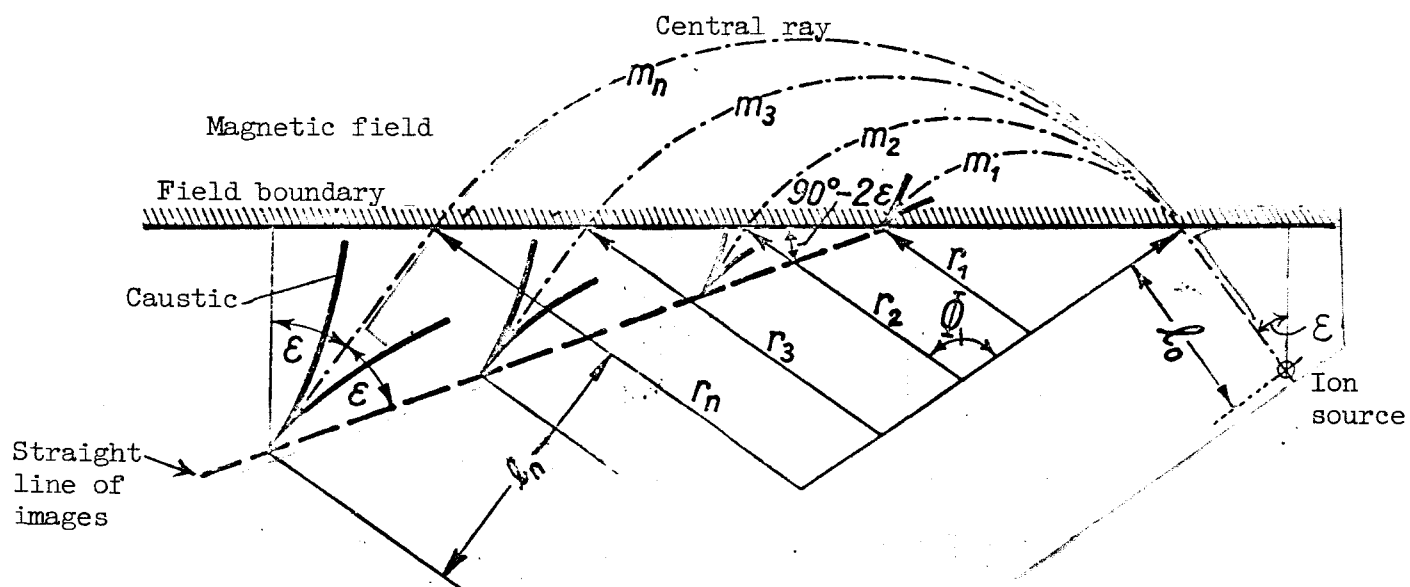
3. It is equipped with four ion detectors so that the accelerating voltage can remain constant during the measurement.

4. All of the electronic equipment is transistorized and miniaturized so that it can easily be housed in the Veronique.

Its main characteristics are the following:

The magnetic induction between the pole pieces	$= 1 \frac{\text{Volt sec}}{\text{m}^2}$
The radius of maximum deviation, i.e., the radius for the orbit of the oxygen molecules	$= 33 \text{ mm}$
The accelerating voltage	$= 2000 \text{ Volts}$
The total weight of the spectrometer with electronic equipment	$= \text{approximately } 30 \text{ kg}$





$\Phi$  = Deflection angle,

$r_n$  = Radius of deviation of the mass  $m_n$ ,

$V$  = Lateral magnification.

$$\cos \Phi = -\frac{1}{3},$$

$$\tan \epsilon = \frac{1}{2} \sqrt{2},$$

$$V = 1 = \text{Constant.}$$

Figure 1. A telescopic system with images on a straight line and with second order aplanatism

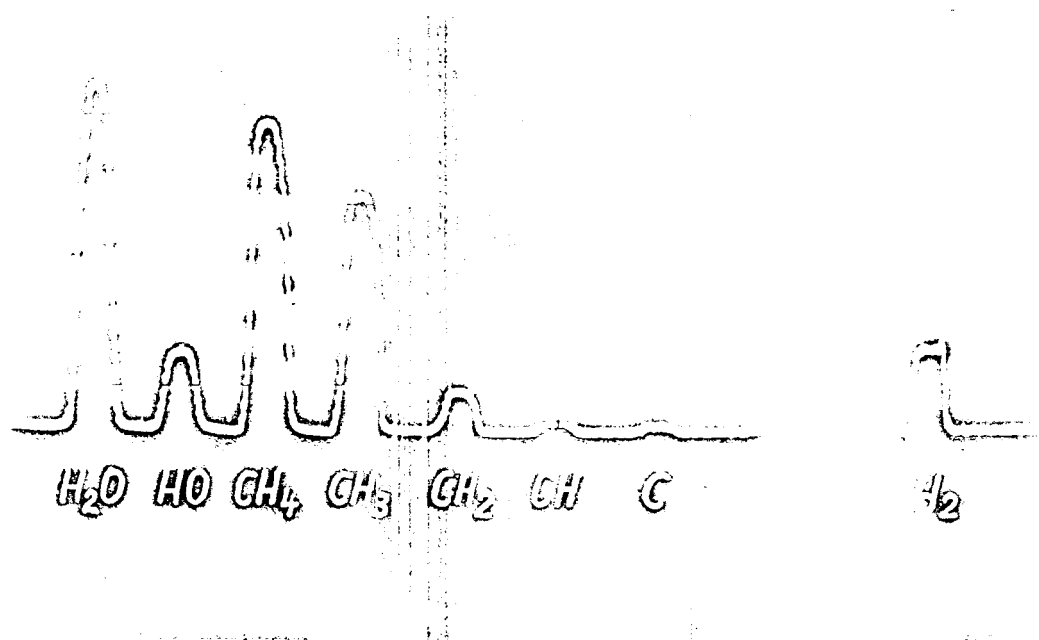


Figure 2. Mass spectrogram of a mixture of  $H_2O-CH_4-H_2$

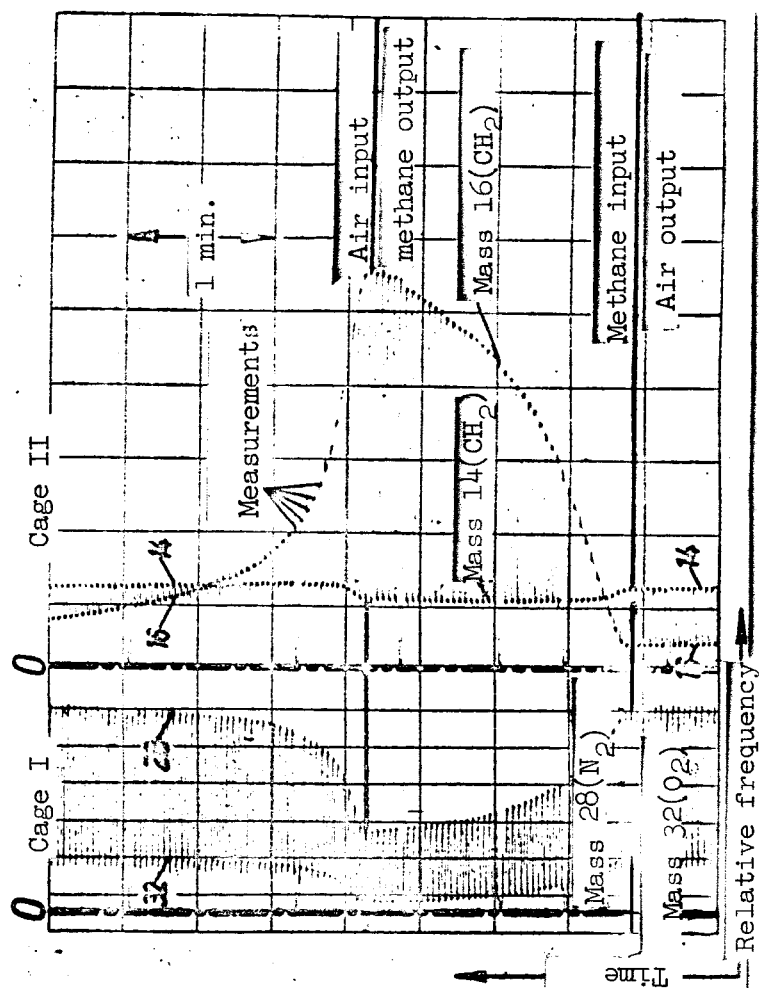


Figure 3. Relative frequencies of the masses 14, 16, 28, 32 of a time-variable mixture of air and methane

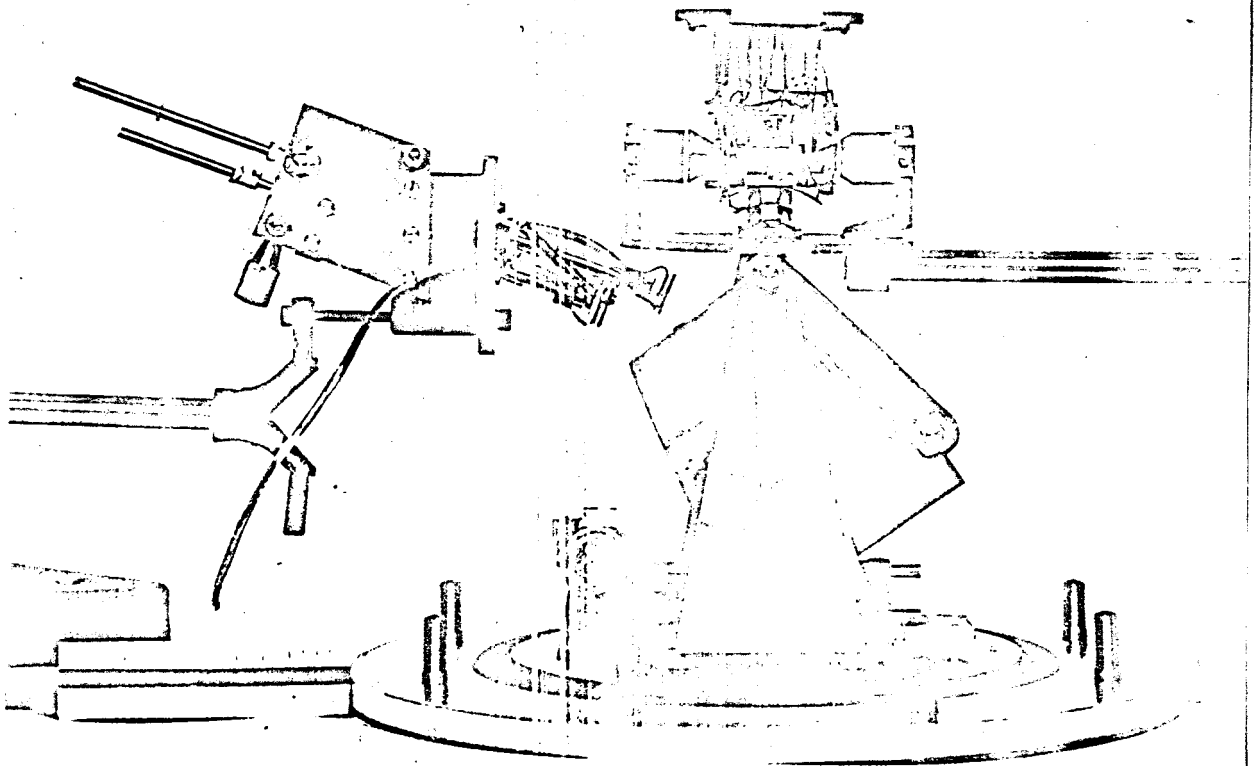


Figure 4. Open view of the prototype showing the ion source; the analyzing magnet; the two detectors

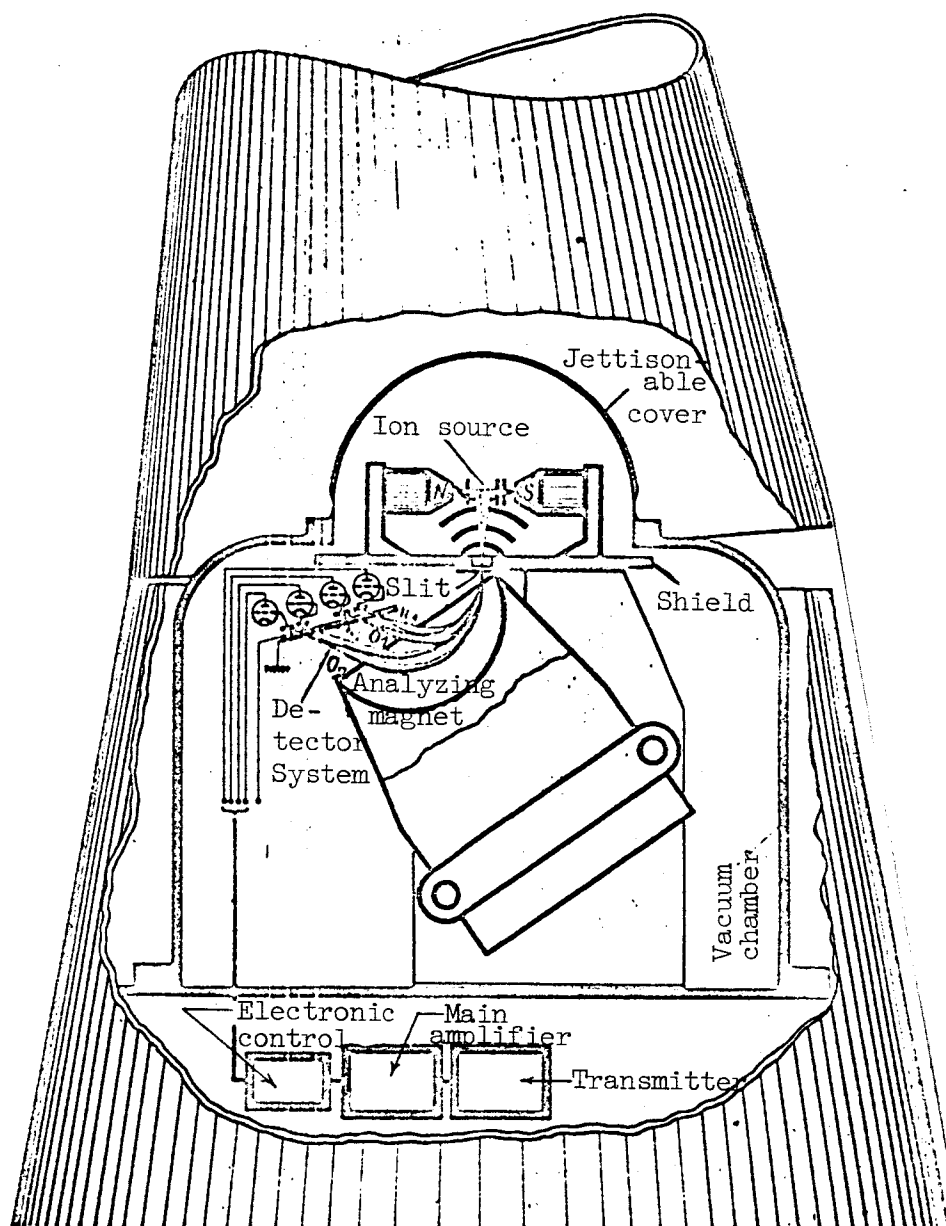


Figure 5. Veronique spectrometer with 4 detectors

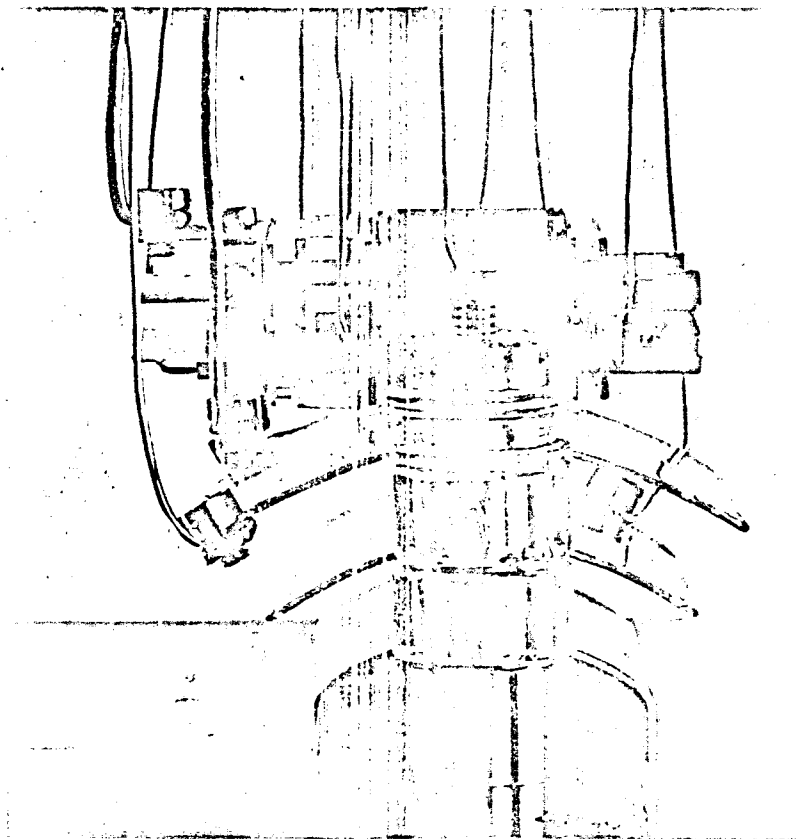


Figure 6. Ion source of the Véronique spectrometer; a) frontal view

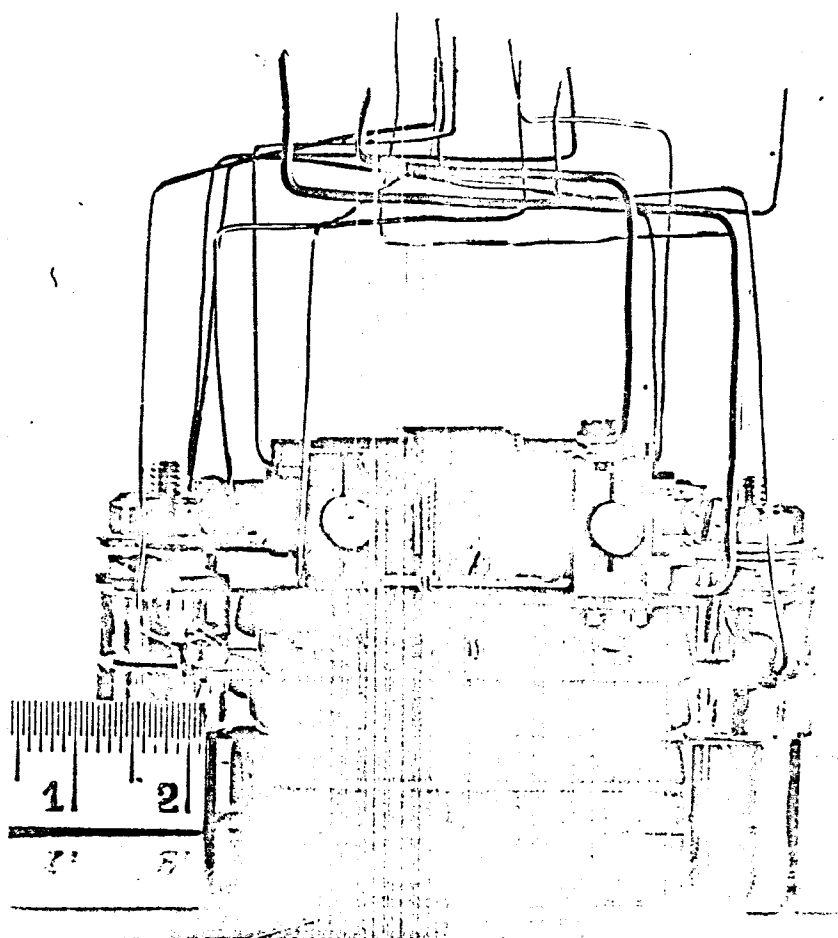


Figure 6b. Side view

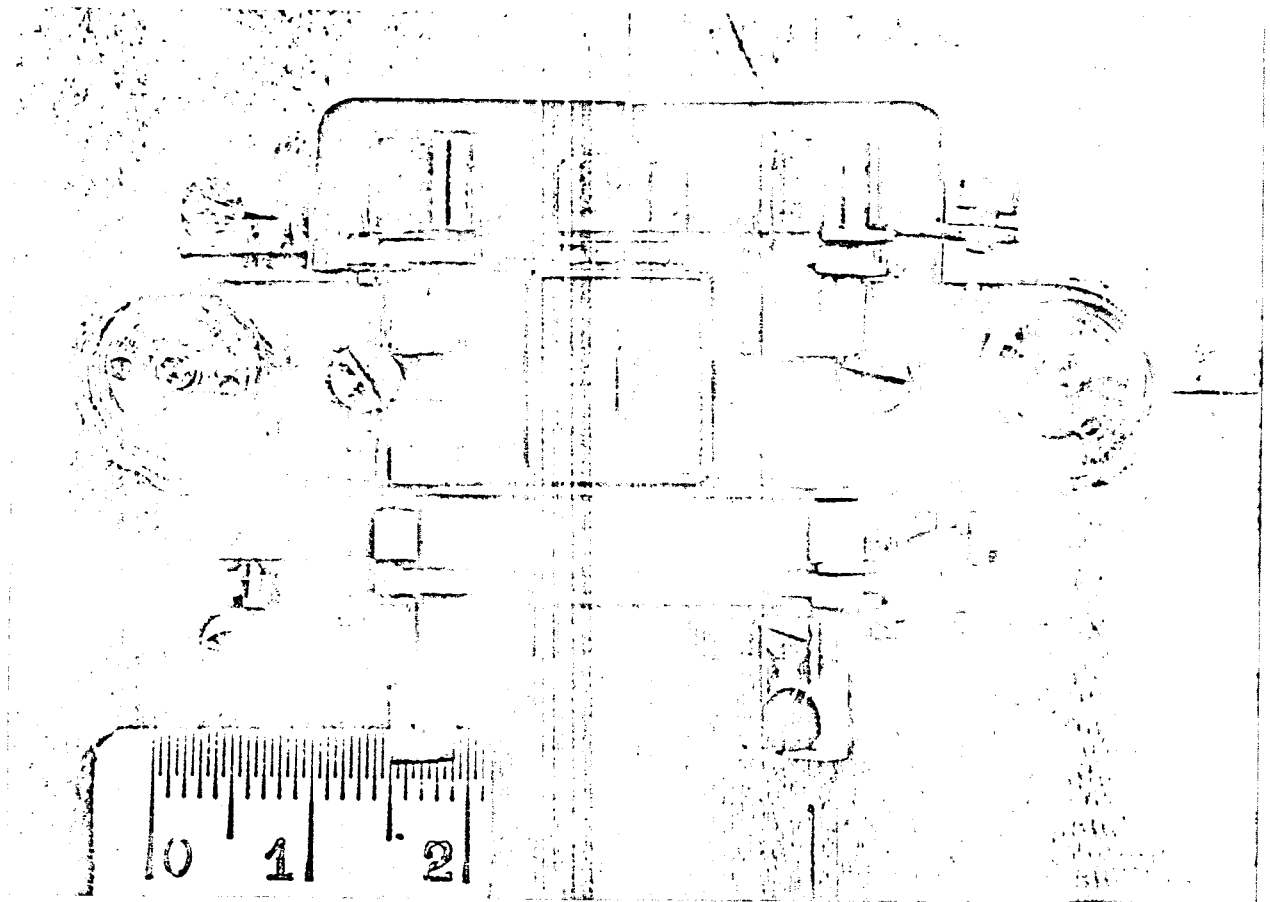


Figure 6c. Top view